Title

Performance Investigations of Two Channel Readout Configurations on the Cross-Strip Cadmium Zinc Telluride Detector.

Journal

IEEE Transactions on Radiation and Plasma Medical Sciences, 8(8)

ISSN

2469-7311

Authors

Enlow, Emily

Wang, Yuli

Shoop, Greyson

et al.

Publication Date

2024-11-01

DOI

10.1109/trpms.2024.3411522

Peer reviewed

HHS Public Access

Author manuscript

IEEE Trans Radiat Plasma Med Sci. Author manuscript; available in PMC 2024 November 12.

Published in final edited form as:

IEEE Trans Radiat Plasma Med Sci. 2024 November ; 8(8): 886–892. doi:10.1109/trpms.2024.3411522.

Performance Investigations of Two Channel Readout Configurations on the Cross-Strip Cadmium Zinc Telluride Detector

Emily Enlow,
Department of Electrical and Computer Engineering, University of California, Santa Cruz, 95064.

Yuli Wang [Student Member, IEEE],
Department of biomedical engineering, Johns Hopkins University, Baltimore, 21204.

Greyson Shoop,
Department of Electrical and Computer Engineering, University of California, Santa Cruz, 95064.

Shiva Abbaszadeh [Senior Member, IEEE]
Department of Electrical and Computer Engineering, University of California, Santa Cruz, 95064.

Abstract

In a detector system where the number of channels exceeds the number of channels available on an application-specific integrated circuit (ASIC), there is a need to configure channels among multiple ASICs to achieve the lowest electronic noise and highest count rate. In this work, two board configurations were designed to experimentally assess which one provides the more favorable performance. In the half-half configuration, contiguous channels from one edge to the center of CZT detector are read by one ASIC, and the other half are read by the other ASIC. In the alternate configuration, the CZT channels are read by alternating ASICs. A lower electronic noise level, better FWHM energy resolution performance (5.35% ± 1.08% compared to 7.84% ± 0.98%), and higher count rate was found for the anode electrode strips with half-half configuration. Cross-talk between ASICs and deadtime play a role in the different performances, and the total count rate of the half-half configuration has a count rate 18.1% higher than that of the alternate configuration.

Index Terms—

Cadmium Zinc Telluride; Cross-strip; ASIC; count rate; electronic noise; energy resolution

I. Introduction

Wide bandgap semiconductor detectors, like cadmium zinc telluride (CZT), can be operated at room temperature and offer high spatial resolution, improved energy resolution, and

This work did not involve human subjects or animals in its research.

high packing fraction (~ 99%) which make them promising detectors for medical imaging modalities such as positron emission tomography (PET) [1]–[4]. The spatial resolution of the semiconductor detector is related to the pitch of the deposited electrodes on the surface of the detector. Two of the most common electrode patterns for CZT detectors are pixelated and cross-strip designs [5]–[9]. The cross-strip design dramatically reduces the number of readout channels [10], when compared to the pixelated electrode CZT detector with similar spatial resolution (2n versus n^2). Previously, ~1 mm spatial resolution of PET systems based on CZT detectors has been demonstrated [2], [11], [12].

To enable low-noise readout electronics, application-specific integrated circuits (ASICs) are commonly used as front-end readout electronics for radiation detectors. When a CZT detector consists of a large number of channels, multiple ASICs are required for one detector. One design consideration is to verify whether the detector electrode to ASIC channel assignment affects the system noise (e.g., through cross-talk of ASIC channels) or count rates. For a system where multiple ASICs are required in one detector, there is a need to configure channels among ASICs to achieve the lowest electronic noise and highest count rate. Utilizing two CZT crystal electrode-to-channel designs in a simulation study, it was previously shown that a configuration where contiguous channels from one edge to the center of CZT detector are read by one ASIC and the other half are read by the other ASIC outperforms a configuration where the channel readouts are alternated between two ASICs [13]. This simulation study showed that when designing a PET system, the electrode-to-channel design has an effect on the electronic noise and count rate and should be considered when developing the readout for semiconductor detectors.

In this work, two board configurations were designed to experimentally assess which one provides the more favorable performance to confirm the previous simulation study [13]. A previous paper from our group reported on the system scale-up of our PET system based on edge-on CZT detectors with a focus on the effect of bonding and stacking of the CZT detectors which uses the half-half configurations [14]. The ASIC used for this study is the RENA-3 (Readout Electronics for Nuclear Applications developed by NOVA R&D Inc., Riverside, CA) which was selected due to its low noise readout, compact design, and number of channels [15]. For both configurations, there are two RENA-3 ASICs and one cross-strip CZT detector. In one configuration, hereafter called half-half configuration, contiguous channels from one edge to the center of the CZT detector are read by one ASIC and the other half are read by the other ASIC. In the second configuration, hereafter called alternate configuration, the CZT channels are read by alternating ASICs. Both these configurations will be tested for energy resolution and count rate using both a test pulse and a point source.

II. Materials and Methods

This section summarizes the design of the CZT detector module and electronic readout system. The system-level characterization and investigation of the two configurations are also described.

A. Cross-strips CZT detector

Fig. 1 (a) shows the design of the CZT detector. Each detector is a monolithic CZT crystal with dimensions of 40 mm × 40 mm × 5 mm. The detectors are used in an edge-on configuration with a length of 40 mm of CZT in the photon path, this leads to an intrinsic sensitivity of 86% for 511 keV photons [16]. Eight cathode electrodes with a 4900 μm width on a 5 mm pitch and 39 anode electrodes with a 100 μm width on a 1 mm pitch are deposited orthogonal to each other on the two opposite 40 mm × 40 mm crystal faces. Thirty-eight steering electrodes are between anodes with the same pitch of 1 mm and a large width of 400 μm. During the experiments, a bias of −600 V and −60 V with respect to anodes was applied to the cathodes and steering electrodes, respectively. When a 511 keV photon interacts with the CZT, an electron-hole pair cloud is generated. The applied bias pulls the electrons to the anode electrodes and the holes to the cathode electrodes. The steering electrode was designed to enhance the anode charge collection. The cross-strip electrode pattern was chosen to use fewer electronic readout channels while still providing high spatial resolution [17].

Two CZT crystals are assembled using flexible circuits based on an anode-cathode-cathode-anode (ACCA) stacking structure to form a 40 mm × 40 mm × 10 mm CZT module (shown in Fig.1 (b)). Conductive silver epoxy is used to facilitate the electrical connections between the CZT crystal and the flexible circuit. The bonding of the CZT and flexible circuits has been studied previously [14]. This ACCA stacking structure decreases the dead space between CZT crystals and increases the packing fraction.

B. Modular readout electronics system

The architecture schematic of the readout electronic system for one panel is shown in Fig. 2. The readout system is comprised primarily of the front-end signal readout part (including the intermediate board and RENA board) and the back-end signal readout part (including the fan-in board and PicoZed board). For the investigation of the two readout configurations on the cross-strip CZT detector, the red dashed box in Fig. 2 shows the data path in the electronic readout system used for the measurements. The experimental setup is shown in Fig. 3.

Each CZT detector has 47 output channels in total (39 anodes and 8 cathodes), which are read by two RENA-3 (Readout Electronics for Nuclear Applications developed by NOVA R&D Inc., Riverside, CA) ASICs. A custom-designed front-end board called a RENA board consists of two RENA-3 ASICs and a Xilinx Spartan 3 field programmable gate array which controls the readout protocol for the RENA-3 ASICs. The intermediate boards provide the connection to high voltage and steering voltages and also define the different readout configurations (half-half or alternate configuration which is presented in detail in II-C) between the CZT detector and the RENA-3 ASIC, which is the focus of this paper.

The fan-in board connects to a 1-column by 30-row array of RENA boards. The fan-in board is responsible for generating the system-wide 50 MHz clock, receiving RENA-3 signals, and distributing the clock and UV signal to all 30 RENA boards. A data acquisition (DAQ) chain, capable of 2 Gbps data transmission, is connected to DAQ computer via an SFP

connector. The DAQ chain was implemented by the Picozed board, which is attached to the backside of the fan-in board.

C. Two intermediate boards with different readout configuration

Two RENA-3 ASICs (36 channels individually) are used to read 39 anodes and 8 cathodes of each CZT detector. Two different readout configurations are applied to anodes: half-half configuration and alternate configuration, which is shown in Fig. 4. Alternate readout configuration was the same used in [2] and [11], where anode 1 was read by RENA-3 ASIC 1 and anode 2 was read by RENA-3 ASIC 2 and so on. In half-half configuration, anode 1 to anode 20 was read by RENA-3 ASIC 1 (half of the CZT crystal) and RENA-3 ASIC 2 readout anode 21 to anode 39. For the cathode readout configuration, the alternate configuration utilizes the same layout used in [2]. A GATE simulation study completed by [13], found that due to the edge-on measurement, the load balance between the two RENA ASICs in the alternating configuration was higher in ASIC 1 than in ASIC 2. For the half-half configuration, the load balance for the cathodes is optimized so that both ASIC 1 and ASIC 2 should carry approximately 50% of the counts.

To achieve the two different readout configurations, two intermediate boards were designed, shown in Fig. 5. Fig. 5 (a) shows the intermediate board with alternate readout configuration, which is with the size of 9.0 cm × 20.9 cm to connect one array of 1×3 CZT crystals to three RENA boards. The intermediate board with half-half configurations is presented in Fig. 5 (b) to connect 1×5 CZT crystals to five RENA boards. The same CZT connectors and RENA connectors are applied to the two intermediate boards, thus we investigate two aforementioned readout configurations by replacing two intermediate boards.

To have a successful operation of the DAQ chain and minimize the time jitters and cross-talk among ASICs channels, the the data acquisition trigger thresholds (V_{thresh}) for the digital to analog converter (DAC) of each channel on each RENA ASIC was optimized manually. We increased the V_{thresh} value of each channel to above the noise level and to prevent the signal triggering by the noise. After completing the adjustment of triggering levels for all ASICs, the system is ready for the measurements. The V_{thresh} value of each channel would be monitored and tuned repeatedly when we adjust the readout electronics of the system.

D. Electronics noise with test pulse

To quantify the internal electronic noise contribution to the energy resolution of the two different intermediate boards (i.e. two different readout configurations), we used a square wave as a test pulse to provide charge injection to each channel. To simulate equivalent charge injection by a 511 keV photon in CZT detector, a square wave with 1 kHz with 250 mV peak-to-peak amplitude without offset was used during the experiment. An example of the experimental setup is shown in Fig. 3, which also presents how different boards are connected. In our studies, data were acquired when:

- CZT detector, intermediate board (with half-half readout configuration or with alternate readout configuration), RENA board and fan-in board are connected together.

- HV bias and steering bias of CZT are turned on.

Each data acquisition time was set as 5 minutes. The experiment was repeated 5 times to get the standard deviation. The same experimental process is applied to the two intermediate boards with different readout configurations with the same CZT and RENA board. During the experiments, the whole system is packaged into a light-tight Faraday cage to reduce interference from outside light and external electronic noise. The results of the spectral peak with full width at half maximum (FWHM) was reported in keV units. The corresponding results are shown in section III-A.

E. Experiments with Ge-68 as the point source

The anode energy resolution and channel count rate are studied based on the edge-on irradiation configuration with a Ge-68 point source. A 170 μCi, 250 μm diameter Ge-68 point source was placed 10 mm away from the center of the 40 mm × 5 mm edge-face of the CZT detector. The anode strips of the CZT detector were oriented toward the point source as described in Fig.2.

Similar to the test pulse experiment, the data acquisition time of each experiment was 5 minutes. The experiment was repeated 5 times to get the standard deviation. The same experimental process is applied to the two intermediate boards with different readout configurations using the same CZT and RENA board for all tests.

The calibration of signal amplitude from ADC units to keV are performed for each anode channel. In Fig. 6, linearity of digitizing photon energy is confirmed by sampling ADC values obtained from multiple sources that emit a wide range of photon energies ranging from 122 keV from Co-57 to 1274 keV from Na-22. By recording the photopeaks in ADC units corresponding to the energy peak at two known energies (Ge-68 for 511 keV and Cs-137 for 662 keV), a linear ADC-to-keV calibration map and the ADC/keV conversion factors for each channel were developed. All results reported in the paper are in keV.

1) Anode energy resolution experiments: The anode energy resolution refers to an energy spectrum containing events of deposited energy to each anode channel, which was acquired from the aforementioned experiment process. The events consist of the photoelectric peak events (511 keV energy deposition in the CZT volume corresponding to a single anode), Compton scatter (a large number of the interaction events will have energy deposition much less than 511 keV, which corresponds to small amplitude signals and is the dominating event in CZT), as well as charge-shared events (when interactions occur in the boundary between two adjacent anodes and the charge is collected on both). We compare the anode energy resolution performance by channels of the two different readout configurations, and the results are summarized in section III-B.

2) Anode count rate investigations: A Python code was developed to count the total events for each anode channel and filter the events of interest between 450 keV and 600 keV from the total events of an anode energy spectrum. To quantitatively analyze the count rate of two different readout configurations, we measured the filtered count rate of each anode channel and the total count rate value of all anode channels for each readout configuration.

III. Results

A. Electronics noise with test pulse

The results of the electronics noise with test pulse using alternate or half-half readout configuration discussed in section II-D are shown in Fig. 7. The summary of energy spectra peak with FWHM in keV units for all 39 anode channels with test pulse is shown in Fig. 8 (a). Fig. 8 (b) presents the energy spectra peak with FWHM in keV units for all 8 cathode channels with test pulse.

The half-half readout configuration produced an average spectra peak with FWHM of 12.61 ± 0.48 keV units (anode) units and 26.16 ± 3.03 keV units (cathode). The average width of the spectra peak broadened to 16.34 ± 1.37 keV units (anode) and 34.45 ± 4.92 keV units (cathode) for alternate readout configuration. Overall, for every readout configuration, anode channels have a lower electronic noise level (smaller average FWHM value of the spectra) than cathode channels. The anode/cathode channels from the half-half readout configuration resulted in a lower electronic noise level (smaller average FWHM value of spectra) than the corresponding anode/cathode channels of alternate readout configuration, which is discussed in section IV in detail.

B. Energy resolution

Fig. 9 (a) and (b) show examples of energy spectra for alternate and half-half readout configurations using Ge-68 as the point source. The lowest detectable energy is around 150 keV. No hole tailing correction was performed on any of the energy spectra for this work. The red curves in both 9 (a) and (b) show a Gaussian fit of the energies between 450 keV and 600 keV, which are events of interest for PET.

The energy resolution (E.R.) was calculated using the Gaussian fit parameter σ to find the full-width half maximum (FWHM) and the center energy of the Gaussian peak (511 keV) via the equations (1) and (2)

$$FWHM = 2\sigma\sqrt{2 * ln(2)} = 2.35\sigma \tag{1}$$

$$E.R. = \frac{FWHM}{511} * 100. \tag{2}$$

The energy resolutions of each anode channel are reported in Fig. 10 for the two different channel configurations. All presented results are without hole tailing correction. From Fig. 10, the average energy resolution for the CZT is 7.84% ± 0.98% for alternate readout configuration and 5.35% ± 1.08% for half-half readout configuration. It is noticeable that the half-half readout configuration has better performance on energy resolution than the alternate readout configuration, which is further discussed in section IV. Additionally, the two ASICs have a small effect on the energy resolution, with the average energy resolution

of ASIC 1 being 7.23% ± 0.58% for the alternating configuration and 4.57% ± for the half-half configuration. ASIC 2 has an average energy resolution of 8.55% ± 0.87% for the alternating configuration and 6.22% ± 0.84% for the half-half configuration.

C. Count rate

According to the method described in section II-E2, we acquired Fig. 11, which shows the total count rate for alternate and half-half configurations. From Fig. 11, it can be seen that the average total count rate for the half-half configuration is 133.9 ± 36.5 kilo-counts, and for the alternate configuration, the average total count rate was 113.4 ± 25.7 kilo-counts. The average filtered count rate, only counting energies between 450 keV and 600 keV, was 32.2 ± 9.0 kilo-counts for the half-half configuration and 29.5 ± 6.2 kilo-counts for the alternating configuration.

IV. Discussion

Work has been done using edge-on CZT cross-strip detectors using the alternate configuration with promising results for preclinical PET systems [2], [10], [11]. Still, a previous simulation study showed a possible improvement by configuring the electrode to channel mapping in the half-half configuration [13]. This work uses the same experimental setup for both configurations except for the intermediate board to allow for a true comparison of the two configurations.

From the internal comparison of Fig. 7 (a) and (b) or Fig. 7 (c) and (d), there is a lower electronic noise from the anode electrodes than that from the cathode electrodes. The width of cathode electrode strips is 8 times larger than the width of anode electrode strips. The larger width of the cathode (~5 mm) in the CZT with 5 mm thickness enables faster triggering and is utilized for timing measurement. The anode channels with widths of 100 μm are used for energy measurement. However, larger widths for the cathode electrodes increase capacitance and dark current. Therefore, a larger electronic noise is expected in the cathode electrode.

All presented data (Fig. 8) were acquired under the same experiment conditions, except for the different readout configurations and the dimensions of the intermediate boards. Since the intermediate board with half-half readout configuration is larger than the board with the alternate readout configuration, a higher electronic noise level should be expected in the intermediate board with the half-half readout configuration. However, from Fig. 8 (a) and (b), we see a lower electronics noise level (small FWHM value) in the half-half readout configuration and higher electronics noise level in alternate readout configuration, for both anode electrodes and cathode electrodes. Therefore, we conclude a much lower electronic noise level of the half-half readout configuration than that of the alternate readout configuration.

From Fig. 10, a better energy resolution performance is shown in the half-half readout configuration. An improvement from 7.84% to 5.35% was observed. The low electronic noise level and reduced crosstalk of the ASICs for the half-half readout configuration when compared to the alternate readout configuration is a major factor in improving

the energy resolution. There was a difference in the energy resolutions between ASIC 1 (non-filled markers) and ASIC 2 (filled markers) for both configurations, with the half-half configuration having a difference of 1.65% while the alternating configuration has a difference of 1.32%. These differences in energy resolution are likely caused by slight differences in the two ASICs.

Compared to the count rate of the alternate configuration, the count rate of the half-half configuration was improved by 18.11% for total counts and 9.43% for filtered counts. For both configurations, the filtered counts accounted for 25% of the total counts during the 5 min tests. Improved count rates were seen for both half-half and alternate configurations for anodes located in the center of the CZT crystal, this is due to the geometry of the test where the point source was centered on the CZT crystal. This improvement in the number of counts can be used in edge-on CZT detectors for Compton-enhanced PET imaging [12], [19].

As previously mentioned in section II-C, the cathode electrodes were optimized to balance the load more evenly between the two ASICs. For the alternating configuration, the cathodes are not optimized, and ASIC 1 accounts for 58.7% of the total counts while ASIC 2 accounts for 41.3% of the total counts. This is in agreement with the previous simulation study [13]. With the cathodes optimized, the half-half configuration had 51.6% of the total counts for ASIC 1 and 48.4% of the total counts for ASIC 2. This confirms the new cathode configuration in the half-half intermediate board leads to a more evenly distributed count rate.

Charge sharing and deadtime are two main factors contributing to the difference in count rates. CZT detectors have carrier density gradient and electrostatic repulsion which causes the induced charge cloud to expand on the path to the collection electrode. In the alternate configuration, after each interaction there is a high probability that both RENAs are triggered and due to the deadtime of both RENAs, the measured count rate becomes smaller than the real counts. In half-half configuration, since charge sharing is read within one RENA, the other RENA is available to detect events. As a consequence, the count rate in half-half is higher and closer to the real counts.

V. Conclusion

In this work, the influence of channel configuration between two ASICs on the electronic noise, FWHM energy resolution, and count rate of a CZT detector with a cross-strip pattern was studied. Lower electronic noise and better FWHM energy resolution were observed in the detector with half-half readout configuration. The FWHM energy resolution for the half-half configuration was found to be 5.35% compared to 7.82% for the alternate configuration. Due to the reduced effects of charge sharing and deadtime, the half-half configuration of anode channels showed a higher count rate than the alternate configuration. With the half-half anode configuration, the total count was 18.44% higher than that of the alternate anode configuration. The load-balanced cathode configuration also improved the count rate between the two ASICs. This study confirms the simulation study performed previously [13] and emphasizes the importance of channel assignment for ASICs to improve both energy resolution and count rate.

Acknowledgment

All authors declare that they have no known conflicts of interest in terms of competing financial interests or personal relationships that could have an influence or are relevant to the work reported in this paper.

The authors acknowledge the support from the National Institute of Biomedical Imaging and Bioengineering of the National Institutes of Health under Award Number R01EB028091.

References

[1]. Zhang F, He Z, Xu D, and Meng L, “Feasibility study of using two 3-D position sensitive CZT detectors for small animal PET,” in IEEE Nuclear Science Symposium Conference Record, 2005, vol. 3, 2005, pp. 1585–1589.

[2]. Gu Y, Matteson J, Skelton R, Deal A, Stephan E, Duttweiler F, Gasaway T, and Levin C, “Study of a high-resolution, 3D positioning cadmium zinc telluride detector for PET,” Physics in Medicine & Biology, vol. 56, no. 6, pp. 1563–1584, 2011. [PubMed: 21335649]

[3]. Zhang F, Herman C, He Z, De Geronimo G, Vernon E, and Fried J, “Characterization of the H3D ASIC readout system and 6.0 cm^3 3-D position sensitive CdZnTe detectors,” IEEE Transactions on Nuclear Science, vol. 59, no. 1, pp. 236–242, 2012.

[4]. Groll A, Kim K, Bhatia H, Zhang JC, Wang JH, Shen ZM, Cai L, Dutta J, Li Q, and Meng LJ, “Hybrid pixel-waveform (HPWF) enabled CdTe detectors for small animal gamma-ray imaging applications,” IEEE Transactions on Radiation and Plasma Medical Sciences, vol. 1, no. 1, pp. 3–14, 2017. [PubMed: 28516169]

[5]. Zhang X, Li F, Hao Y, Bai R, Xin Y, Sun Q, Ouyang X, Jie W, and Xu Y, “Improved energy resolution by weighting potential optimization in CsPbBr3 pixelated gamma-ray detector,” IEEE Transactions on Electron Devices, vol. 70, no. 10, pp. 5190–5195, 2023.

[6]. Hu H, Niu G, Zheng Z, Xu L, Liu L, and Tang J, “Perovskite semiconductors for ionizing radiation detection,” EcoMat, vol. 4, no. 6, p. e12258, 2022.

[7]. Yin Y and Komarov S, “Positron emission tomography (PET) imaging based on sub-millimeter pixelated CdZnTe detectors,” Advanced X-ray Detector Technologies: Design and Applications, pp. 261–286, 2022.

[8]. Li Y, Pei C, Liu M, Wen J, Zhang Q, Huang C, Yin Y, Li G, and Chen X, “Characterization of 1mm cross-strip 3D CZT detectors for PET imaging application,” in 2021 IEEE Nuclear Science Symposium and Medical Imaging Conference (NSS/MIC), 2021, pp. 1–4.

[9]. Altıngün AM and Kalemci E, “Optimization study of the electrode design of a 5 mm thick orthogonal-strip CdZnTe detector system,” Nuclear Instruments and Methods in Physics Research Section A: Accelerators, Spectrometers, Detectors and Associated Equipment, vol. 1027, p. 166125, 2022.

[10]. Gu Y and Levin CS, “Study of electrode pattern design for a CZT-based PET detector,” Physics in Medicine Biology, vol. 59, no. 11, pp. 2599–2621, May 2014. [PubMed: 24786208]

[11]. Abbaszadeh S, Gu Y, Reynolds PD, and Levin CS, “Characterization of a sub-assembly of 3D position sensitive cadmium zinc telluride detectors and electronics from a sub-millimeter resolution PET system,” Physics in Medicine Biology, vol. 61, no. 18, pp. 6733–6753, Aug 2016. [PubMed: 27551981]

[12]. Jin Y, Streicher M, Yang H, Brown S, He Z, and Meng L-J, “Experimental evaluation of a 3-D CZT imaging spectrometer for potential use in Compton-enhanced PET imaging,” IEEE Transactions on Radiation and Plasma Medical Sciences, vol. 7, no. 1, pp. 18–32, 2023. [PubMed: 38106623]

[13]. Li M and Abbaszadeh S, “Influence of channel configuration on bandwidth of cadmium zinc telluride detector with a cross-strip pattern,” Radiation Physics and Chemistry, vol. 155, pp. 213–216, 2019.

[14]. Enlow E, Diba M, Clayton J, Harris B, and Abbaszadeh S, “Impact of flexible circuit bonding and system integration on energy resolution of cross-strip CZT detectors,” IEEE Transactions on Radiation and Plasma Medical Sciences, vol. 7, no. 6, pp. 580–586, 2023. [PubMed: 38468608]

[15]. Cajipe VB, Clajus M, Hayakawa S, Matteson JL, Skelton RT, Tumer TO, and Volkovskii A, "Performance of the RENA-3 IC with position-sensitive CZT and CdTe detectors," in 2008 IEEE Nuclear Science Symposium Conference Record, 2008, pp. 300–307.

[16]. Habte F, Foudray AMK, Olcott PD, and Levin CS, "Effects of system geometry and other physical factors on photon sensitivity of high-resolution positron emission tomography," Physics in Medicine Biology, vol. 52, no. 13, pp. 3753–3772, May 2007. [PubMed: 17664575]

[17]. Maehlum G, Dietzel KI, Meier D, Szawlowski M, Sundal B, Vandehei T, Wagenaar D, and Patt BE, "Study of cadmium zinc telluride (CZT) radiation detector modules under moderate and long-term variations of temperature and humidity," in 2007 IEEE Nuclear Science Symposium Conference Record, vol. 2, 2007, pp. 1645–1648.

[18]. Wang Y, Herbst R, and Abbaszadeh S, "Development and characterization of modular readout design for two-panel head-and-neck dedicated PET system based on CZT detectors," IEEE Transactions on Radiation and Plasma Medical Sciences, vol. 6, no. 5, pp. 517–521, 2022. [PubMed: 37711549]

[19]. Yoon C and Lee W, "Advanced PET using both Compton and photoelectric events," Journal of the Korean Physical Society, vol. 61, pp. 626–629, 2012.

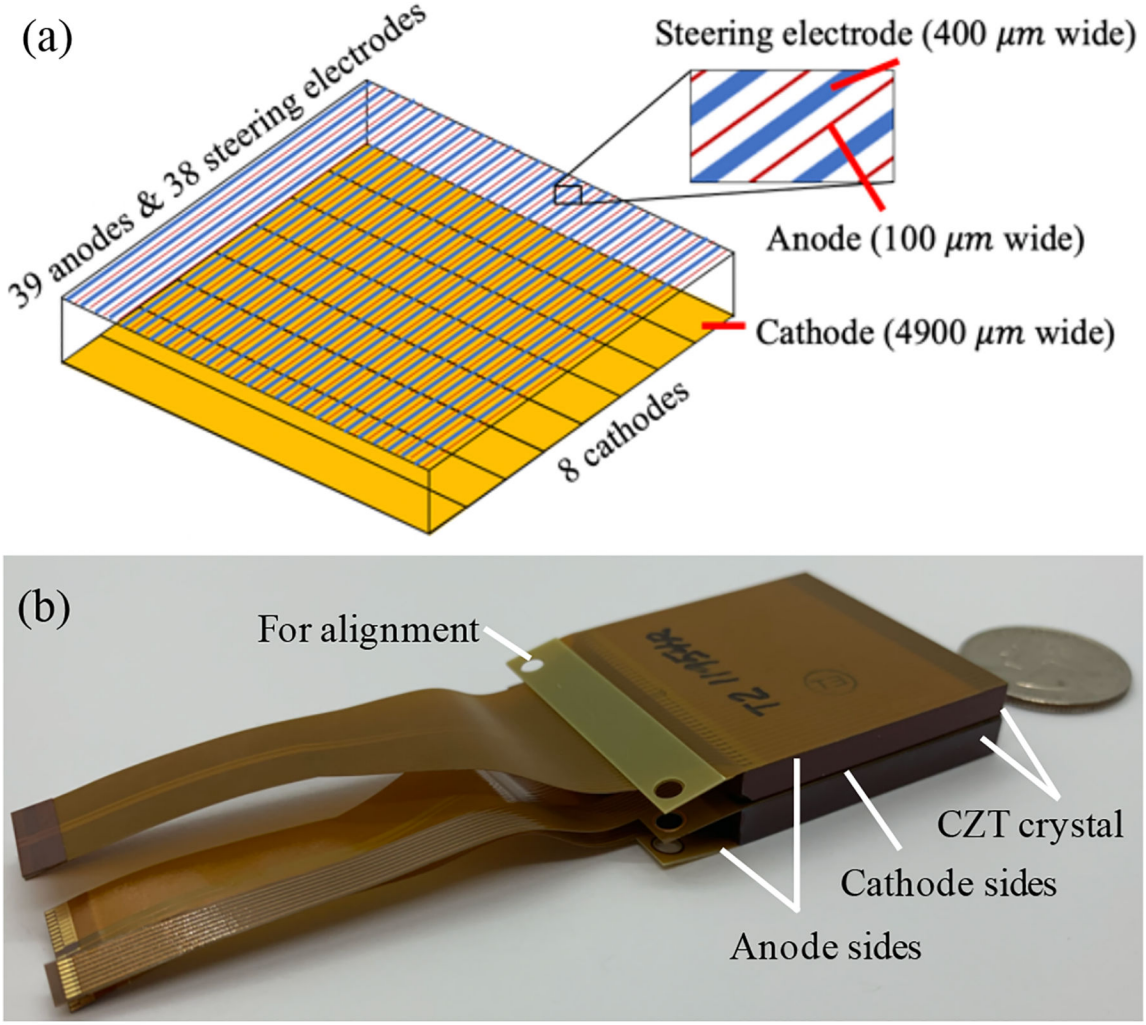

Fig. 1.

(a) Schematic of CZT crystal with cross-strip electrode pattern showing anodes, cathodes, and steering electrodes. (b) Two CZT are assembled with flexible circuits and stacked based on anode-cathode-cathode-anode configuration to form a CZT module (4 cm × 4 cm × 1 cm).

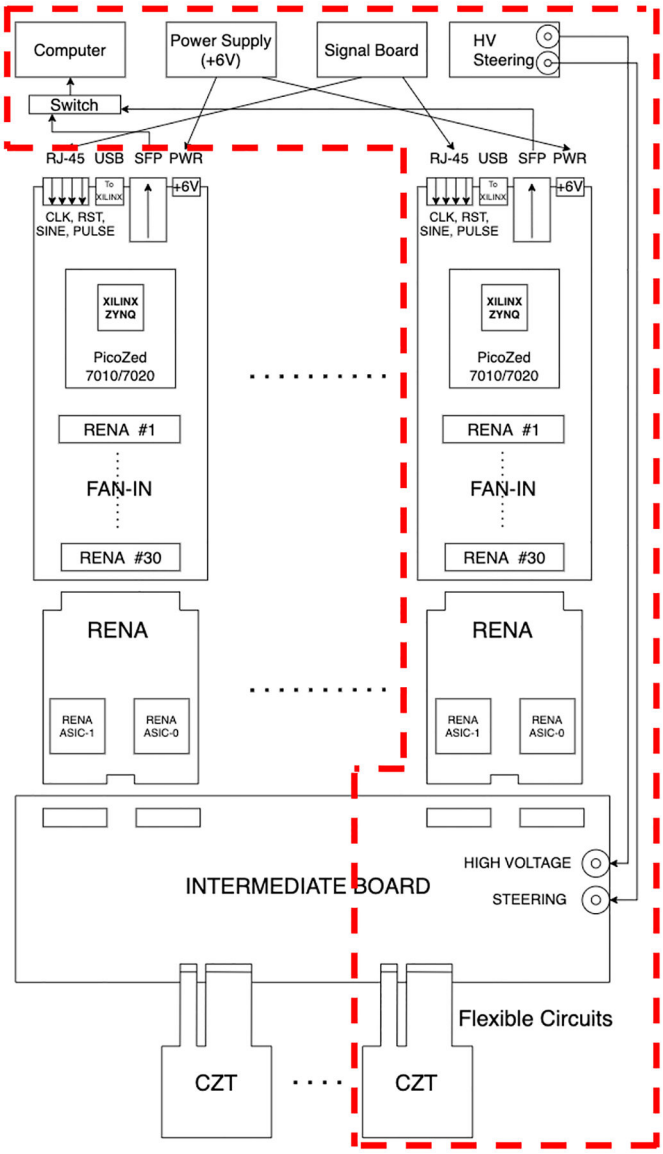

Fig. 2.

Architecture of the DAQ chain of one panel for the head and neck PET system. The red dashed box marks one datapath for one of the modular DAQ electronics. Five modular DAQ electronics form the DAQ chain of one panel [18].

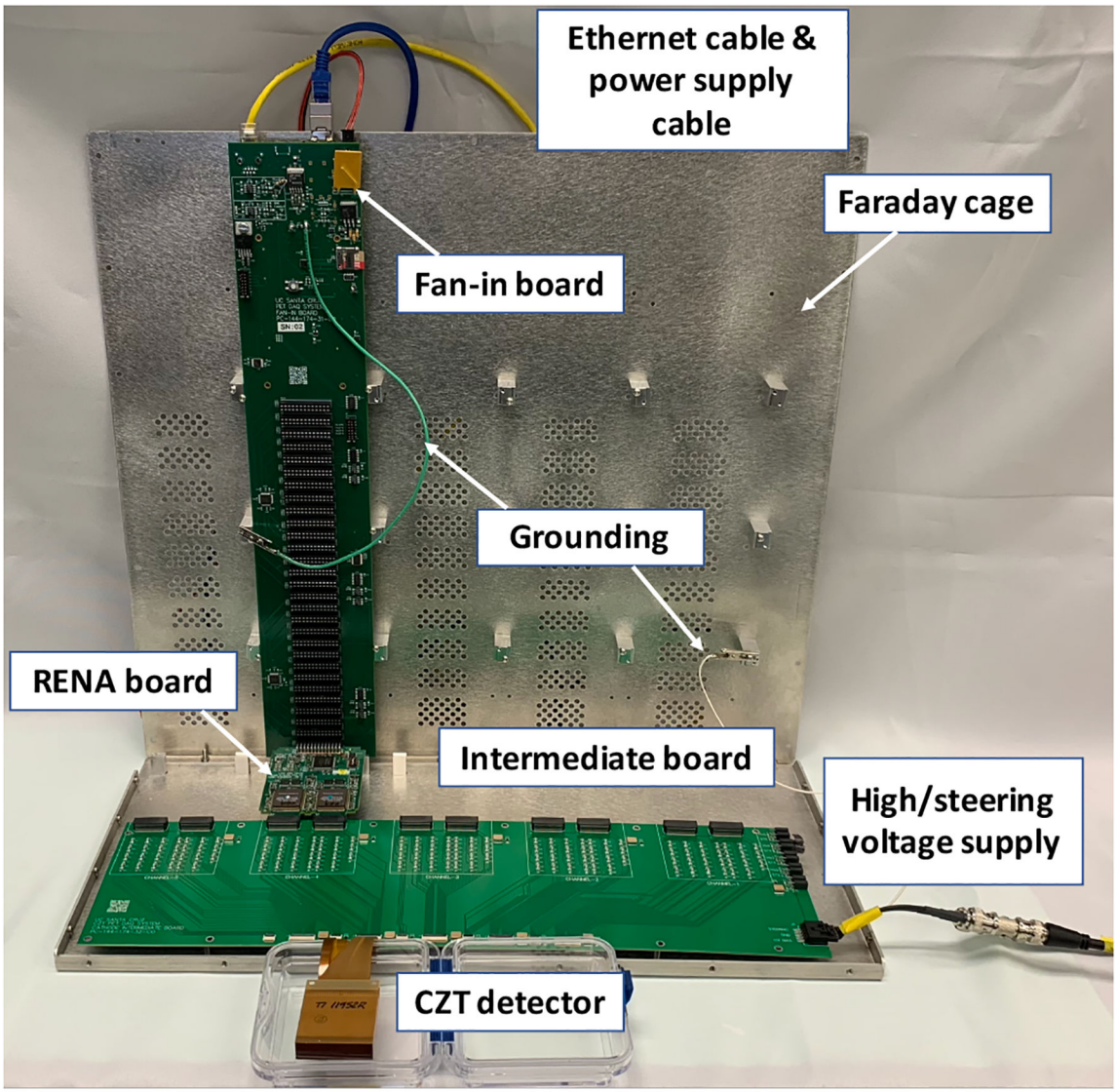

Fig. 3.
An example picture of the experimental setup with the half-half intermediate board in place.

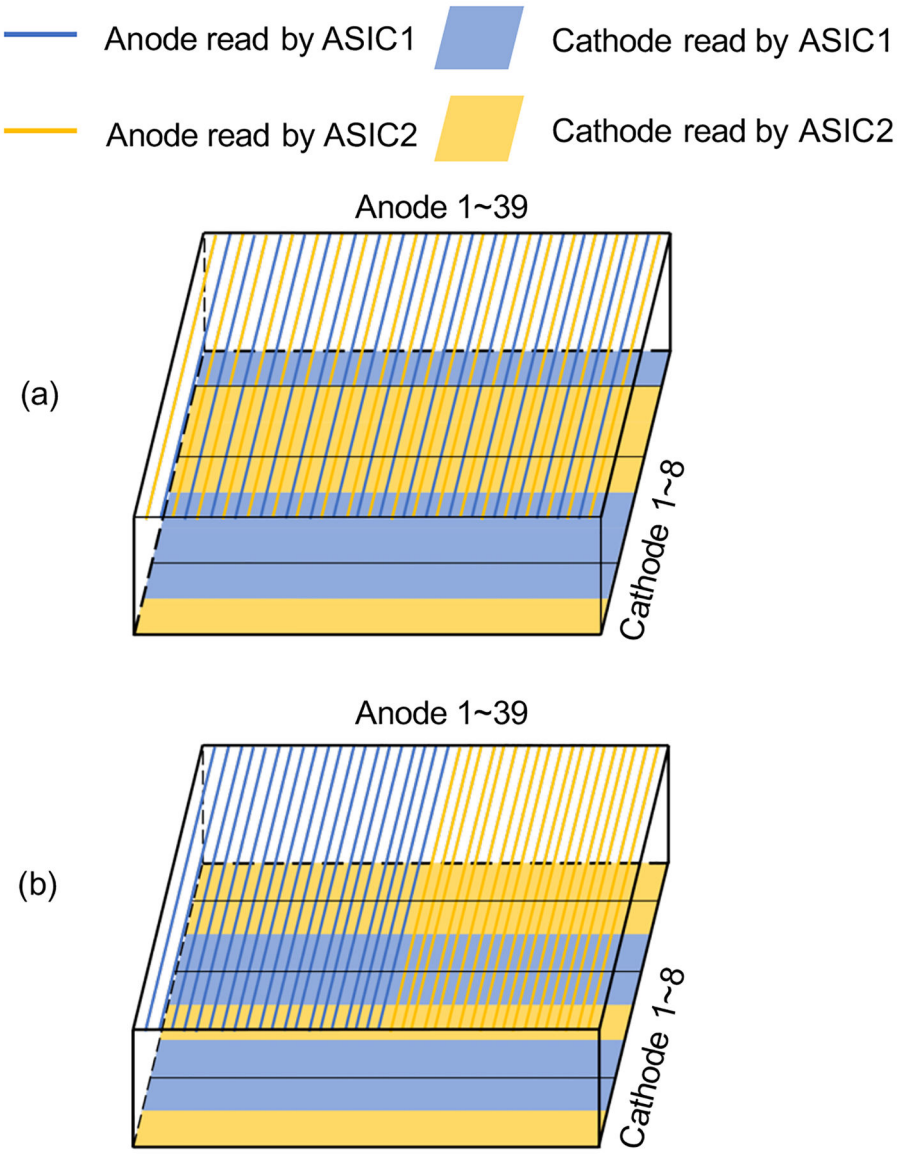

Fig. 4.

Schematic of one CZT electrodes distribution to two RENA-3 ASICs readout (a) previous design and for (b) new design in this paper. (a) For previous design, anodes have the alternate configuration between two RENA-3 ASICs. (b) For new design, anodes have the half-half configuration where anode 1 to anode 20 are read out with RENA-3 ASIC 1 and the anode 21 to anode 39 are readout with RENA-3 ASIC 2.

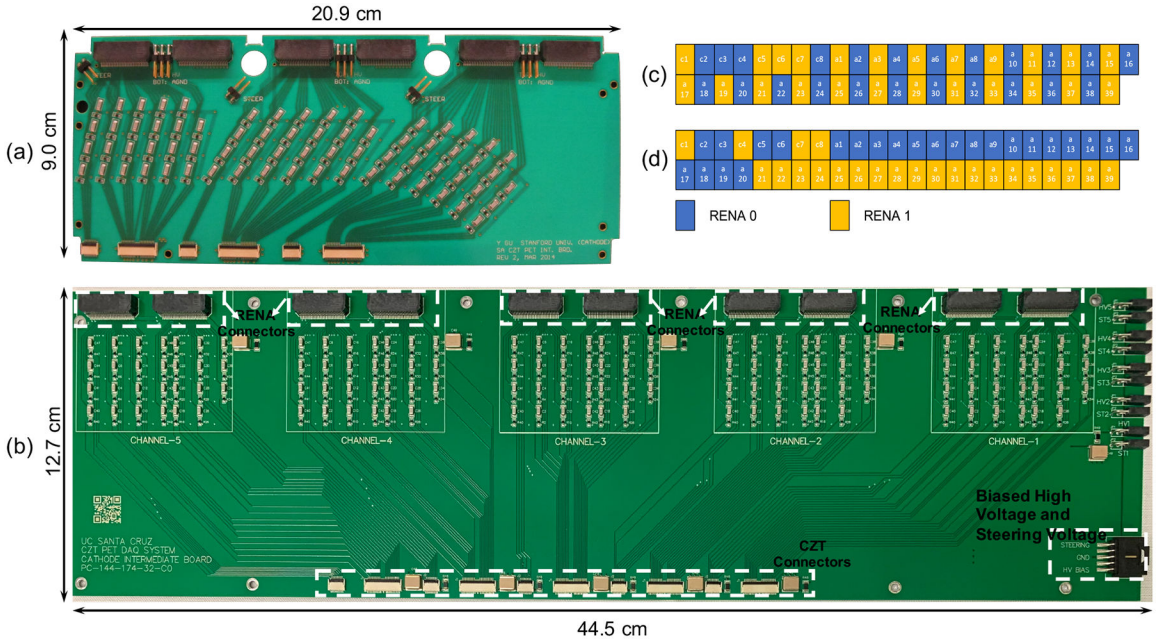

Fig. 5.

(a) Schematics of the intermediate board with alternate readout configuration with dimensions of 9.0 cm × 20.9 cm. (b) Schematics of the intermediate board with half-half readout configuration with dimensions of 12.7 cm × 44.5 cm. (c) Channel distribution map between RENA ASICs and CZT anode/cathode readout channels for alternate readout configuration. (d) Channel distribution map between RENA ASICs and CZT anode/cathode readout channels for half-half readout configuration. RENA0 is ASIC 1 and RENA1 is ASIC 2.

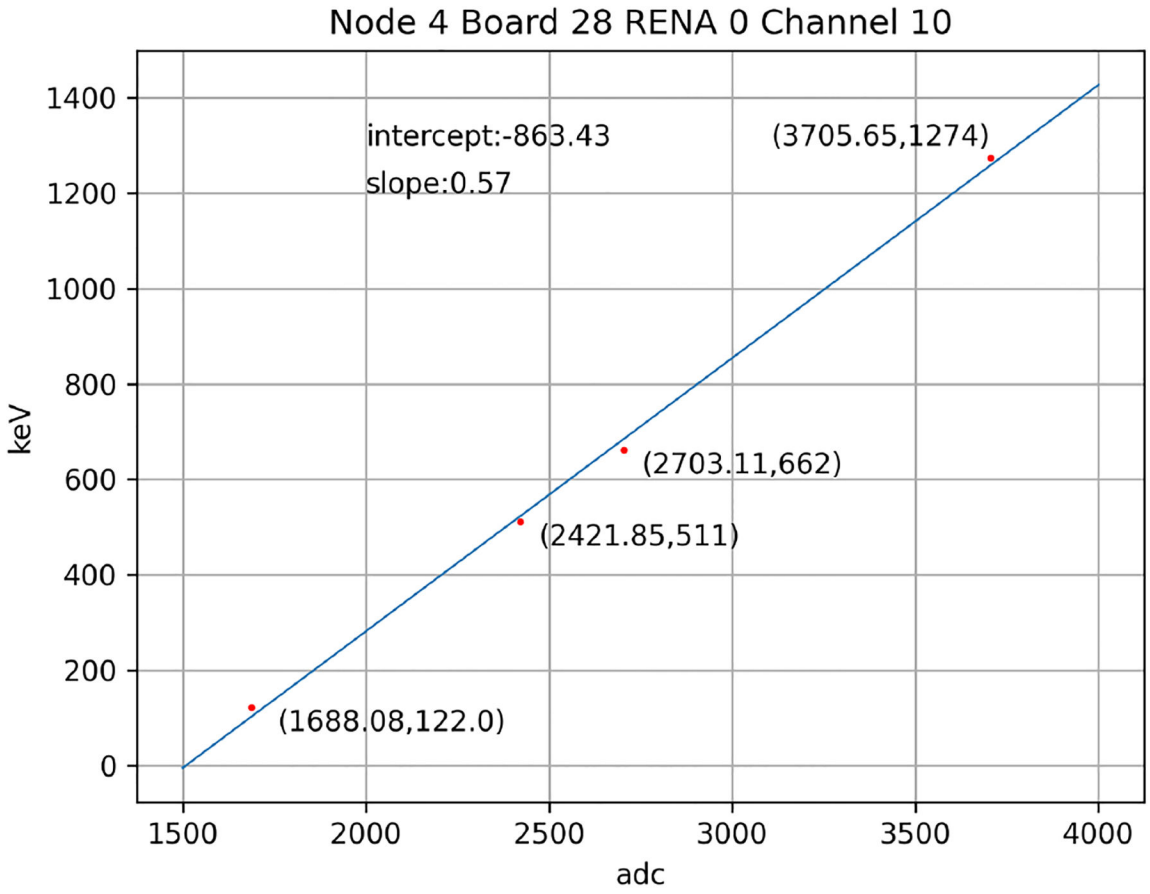

Fig. 6.

Linear fit of digitizing photon energy in keV to ADC units. Energies from Co-57, Ge-68, Cs-137, and Na-22 are sampled in ADC units and a linear regression is performed to demonstrate linearity over a wide range (122 – 1274 keV).

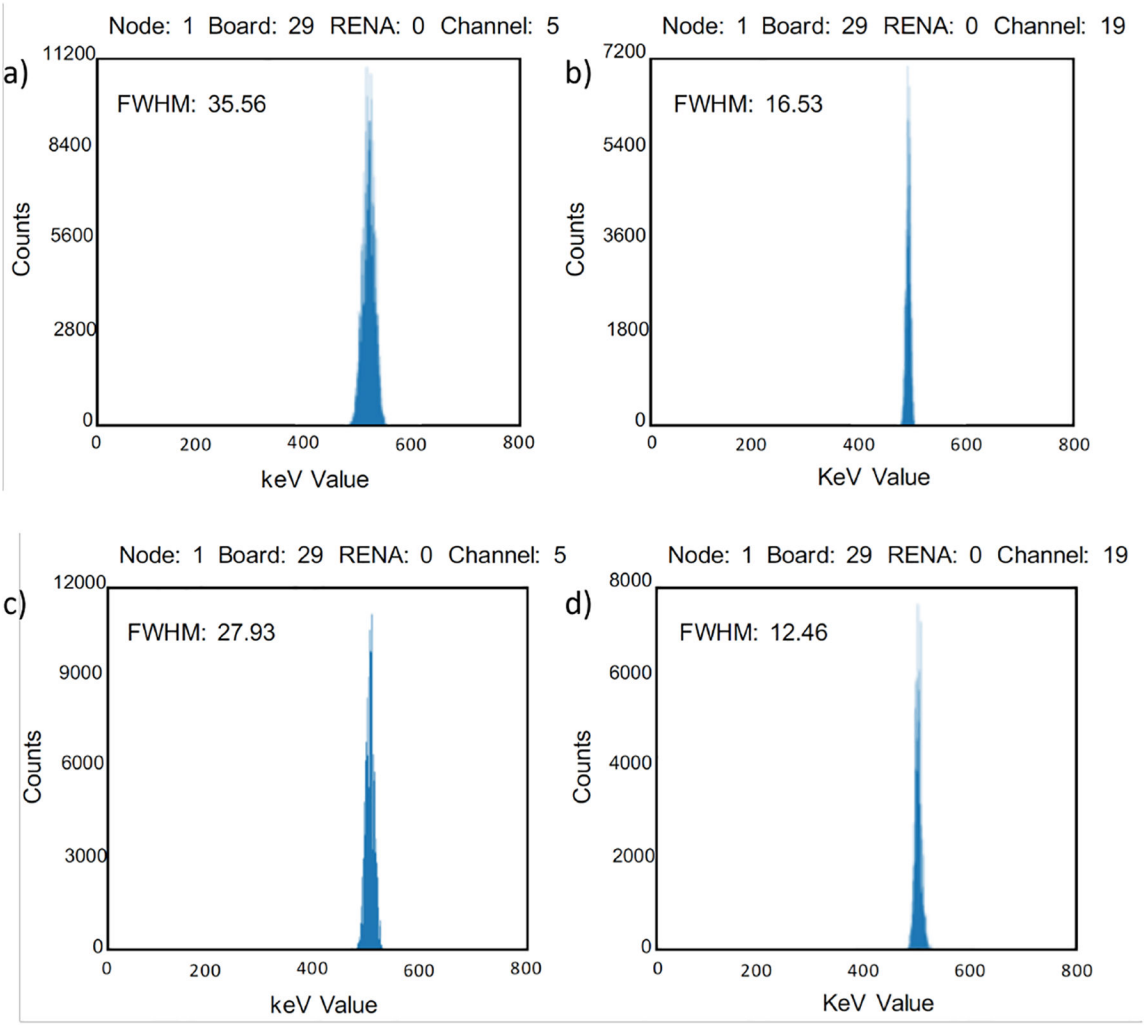

Fig. 7.

Results examples of energy resolution with test pulse for alternate readout configuration in (a) cathode channel and (b) anode channel. Results examples of energy resolution with test pulse for half-half readout configuration in (c) cathode channel and (d) anode channel

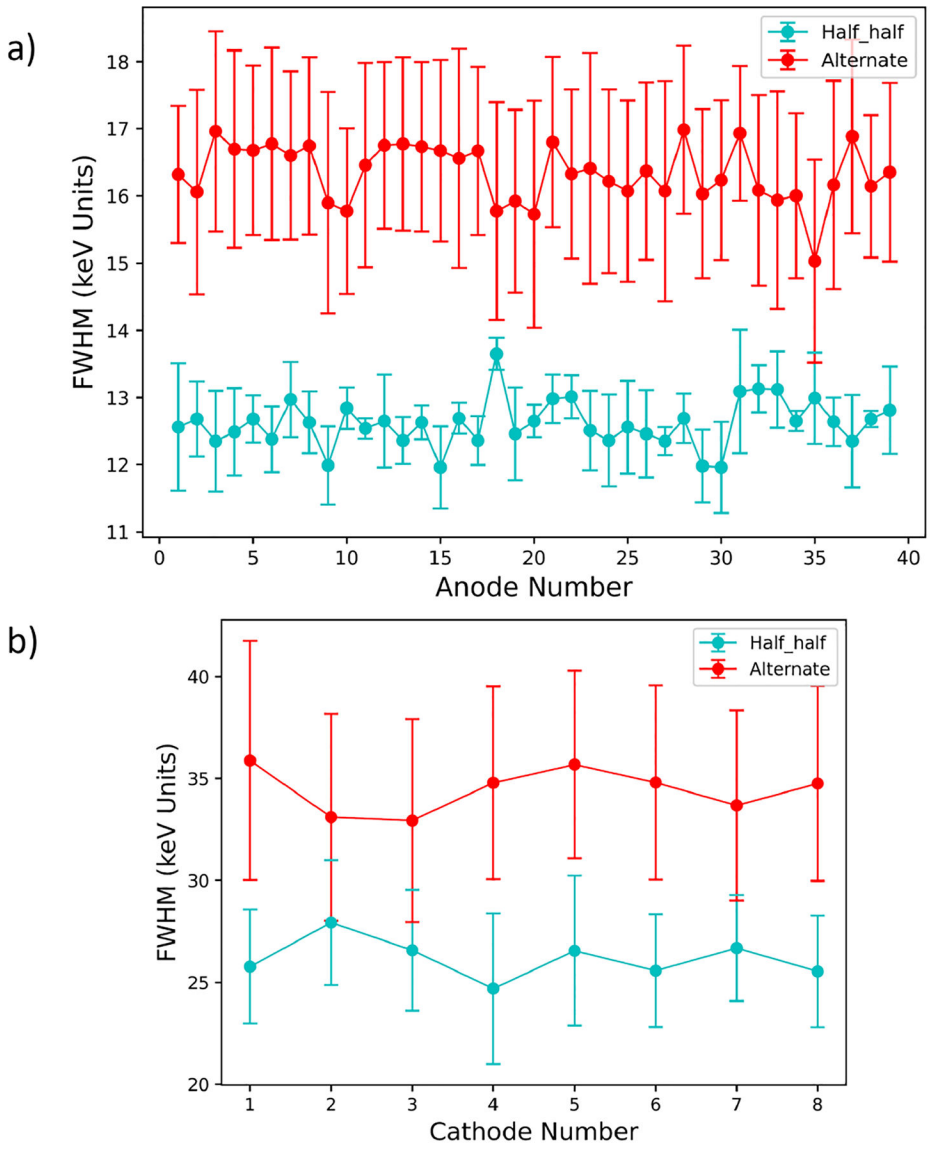

Fig. 8.

(a) Test pulse energy resolution comparison for 30 anode channels between alternate readout configuration and half-half readout configuration. (b) Test pulse energy resolution comparison for cathode channels between alternate readout configuration and half-half readout configuration.

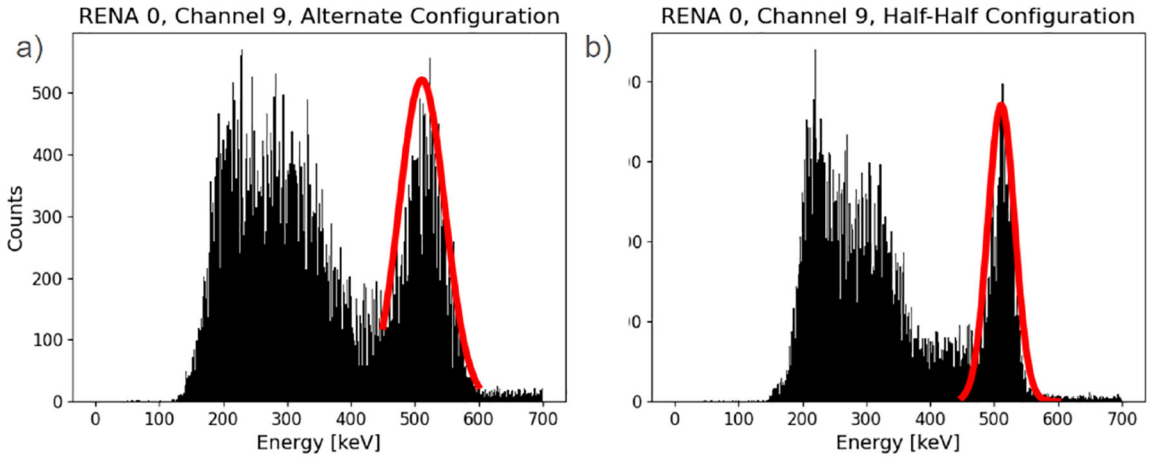

Fig. 9.

Example of one channel energy spectra plot using Ge-68 point source with a red line for the Gaussian fit for (a) alternate readout configuration and (b) half-half readout configuration.

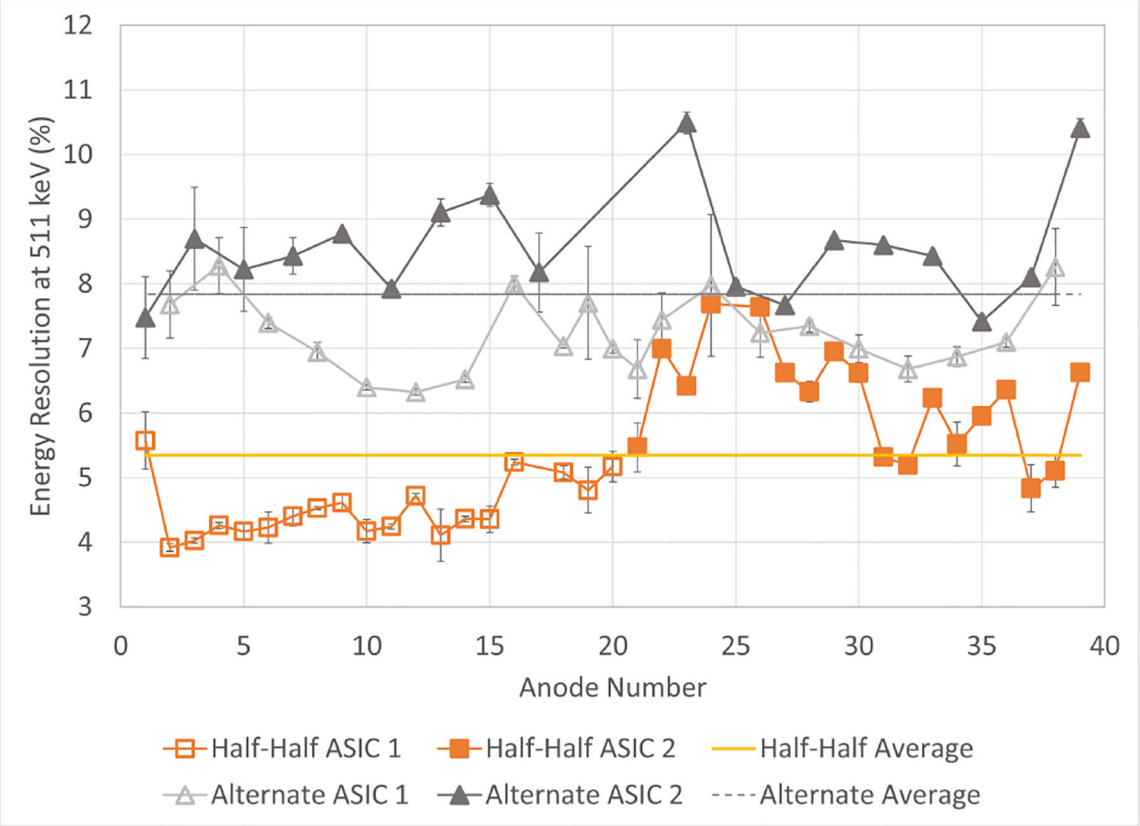

Fig. 10.

Summary of energy resolution as a function of anode number for half-half readout configuration (non-filled orange squares for ASIC 1, filled orange squares for ASIC 2) and alternate readout configuration (non-filled gray triangles for ASIC 1, filled for ASIC 2). The average energy resolutions over the entire CZT are also represented as lines on the figure: half-half (orange solid line), and alternate (gray dotted line).

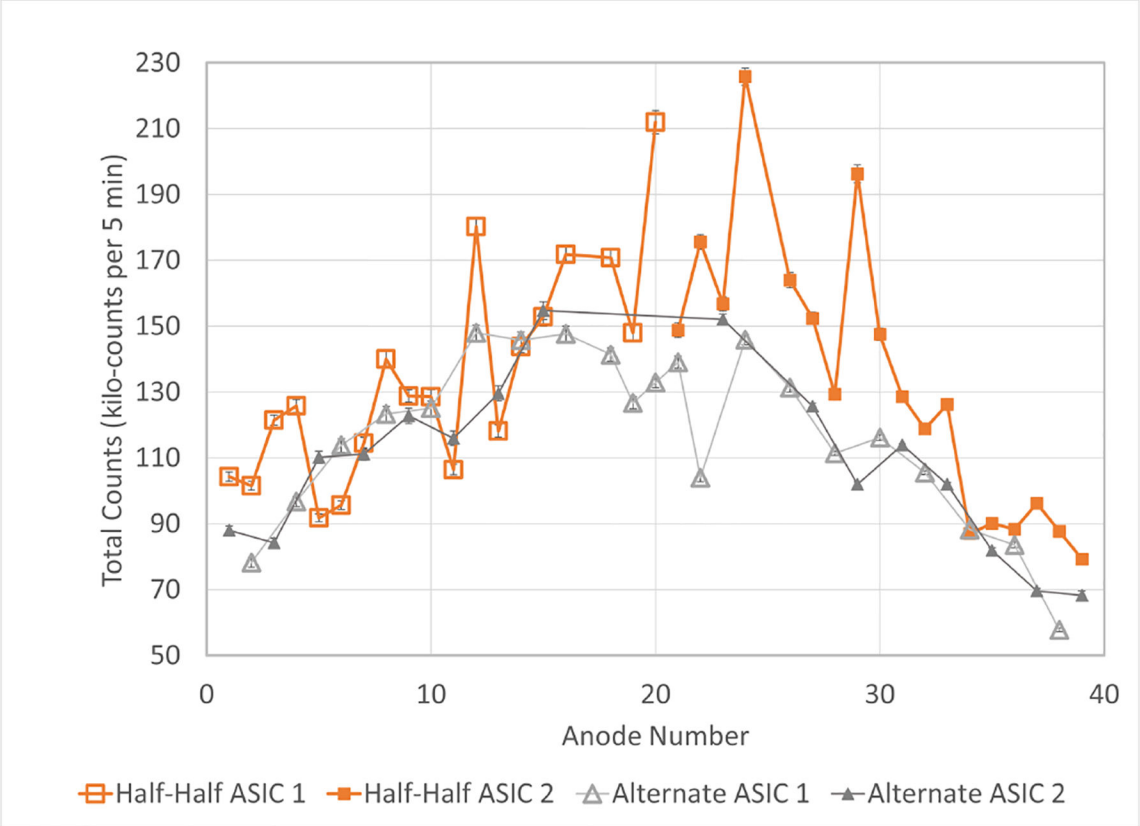

Fig. 11.

Total count rate (kilo-counts per 5 min) as a function of anode number for both half-half readout configuration (non-filled orange square for ASIC 1, filled orange square for ASIC 2) and alternate readout configuration (non-filled gray triangle for ASIC 1, filled gray triangle for ASIC 2).